第 30 卷第 2 期
2014 年 2 月

无 机 化 学 学 报
CHINESE JOURNAL OF INORGANIC CHEMISTRY

Vol.30 No.2
431-441

$BiOI/Bi_2WO_6$ 对甲基橙和苯酚的光催化降解及光催化机理

崔玉民[1,2] 洪文珊[1] 李慧泉*[,1,2] 吴兴才*[,3] 凡素华[1] 朱良俊[1]

([1]阜阳师范学院化学化工学院,阜阳 236037)

([2]安徽环境污染物降解与监测省级实验室,阜阳 236037)

([3]南京大学化学系介观化学教育部重点实验室,配位化学国家重点实验室,南京 210093)

摘要: 采用简单的沉积方法制备了不同碘化氧铋含量的 $BiOI/Bi_2WO_6$ 光催化剂, 通过 X 射线衍射 (XRD)、扫描电子显微镜(SEM)、高分辨透射电子显微镜(HR-TEM)、紫外–可见漫反射光谱(UV-Vis DRS)和 BET 比表面积测量对其进行了表征。在紫外和可见光的照射下, 使用甲基橙和苯酚的光催化降解评价了 $BiOI/Bi_2WO_6$ 催化剂的光催化性能。结果表明: 与商业 P25 和纯 Bi_2WO_6 相比,13.2% $BiOI/Bi_2WO_6$ 光催化剂具有更高的紫外和可见光催化性能。这明显增加的光催化活性主要归功于光生电子和空穴在 Bi_2WO_6 和 BiOI 界面上的有效转移,降低了电子–空穴对的复合。基于 BiOI 和 Bi_2WO_6 的能带结构,提出了光生载流子的一种转移过程。自由基清除剂的实验表明,·OH,h^+,$\cdot O_2^-$和 H_2O_2,特别是 h^+,共同支配了甲基橙和苯酚的光催化降解过程。

关键词: 沉积法; $BiOI/Bi_2WO_6$; 光催化; 甲基橙; 苯酚

中图分类号: O634 **文献标识码**: A **文章编号**: 1001-4861(2014)02-0431-11

DOI: 10.11862/CJIC.2014.001

Photocatalytic Degradation and Mechanism of $BiOI/Bi_2WO_6$ toward Methyl Orange and Phenol

CUI Yu-Min[1,2] HONG Wen-Shan[1] LI Hui-Quan*[,1,2] WU Xing-Cai*[,3] FAN Su-Hua[1] ZHU Liang-Jun[1]

([1]*School of Chemistry and Chemical Engineering, Fuyang Normal College, Fuyang, Anhui* 236037, *China*)

([2]*Anhui Provincial Key Laboratory for Degradation and Monitoring of Pollution of the Environment, Fuyang, Anhui* 236037, *China*)

([3]*Key Laboratory of Mesoscopic Chemistry of MOE, The State Key Laboratory of Coordination Chemistry, School of Chemistry and Chemical Engineering, Nanjing University, Nanjing* 210093, *China*)

Abstract: $BiOI/Bi_2WO_6$ photocatalysts with various BiOI amounts were prepared by a simple deposition method and characterized by X-ray diffraction (XRD), scanning electron microscopy (SEM), high-resolution transmission electron microscopy (HR-TEM), UV-Vis diffuse reflectance spectroscopy (UV-Vis DRS) and low temperature nitrogen adsorption. The photocatalytic performance of $BiOI/Bi_2WO_6$ catalysts was evaluated using the photodegradation of methyl orange (MO) and phenol in an aqueous solution under UV and visible light irradiation. The results indicate that compared with commercial Degussa P25 and pure Bi_2WO_6, the 13.2% $BiOI/Bi_2WO_6$ photocatalyst shows much higher UV and visible light photocatalytic performance. The obviously increased photocatalytic activity could be mainly attributed to the effective transfer of the photogenerated electrons and holes at the interface of Bi_2WO_6 and BiOI, which reduces the recombination of electron-hole pairs. A transfer process of photogenerated carriers is proposed based on the band structures of BiOI and Bi_2WO_6. Radical scavengers experiments demonstrate that ·OH, h^+, $\cdot O_2^-$ and H_2O_2, especially h^+, together dominate the photodegradation process of MO and phenol.

Key words: deposition method; $BiOI/Bi_2WO_6$; photocatalysis; methyl orange; phenol

收稿日期:2013-05-03。收修改稿日期:2013-10-08。

国家自然科学基金(No.21201037),安徽省高校省级自然科学研究项目(KJ2012A217)及环境污染物降解与监测省级实验室校级专项(2012HJJC01ZD)资助项目。

*通讯联系人。E-mail:huiquanli908@163.com,Fax:+865582596703

0 Introduction

The photocatalytic technology has attracted extensive attention due to its applications in wastewater treatment and purification of air [1-4]. The semiconductor TiO_2 has been considered as one of the best photocatalysts owing to its nontoxicity, chemical stability, good photoactivity and low cost[5-8]. However, only a small UV fraction of solar light (3%~5%) can be utilized due to the wide band-gap energy of TiO_2. Therefore, it is urgent to develop highly efficient photocatalysts for pollutants degradation under visible light irradiation. Recently, as one of the new non-titania photocatalysts, Bi_2WO_6 has been widely used for degradation of pollutants under visible light irradiation [9-14]. However, pure Bi_2WO_6 has shown photoabsorption property with wavelength shorter than ~450 nm and high recombination of photo-generated electronhole pairs [9-10]. These two main drawbacks considerably limit the application of Bi_2WO_6. In order to overcome the two drawbacks, combining Bi_2WO_6 with narrow band gap semiconductor has been explored in recent years[15-16].

BiOI has strong photoabsorption ability in 400~700 nm light region, and it has a narrow band-gap energy (~1.8 eV)[17]. In 2012, Chen et al[18]. reported that $Bi_2O_2CO_3$/BiOI heterostructures presented obviously higher visible light photocatalytic activity than that of BiOI or $Bi_2O_2CO_3$, and the enhanced photocatalytic property of $Bi_2O_2CO_3$/BiOI heterostructures could be attributed to its strong absorption in the visible light region and low recombination rate of the electron-hole pairs owing to the heterojunction formed between $Bi_2O_2CO_3$ and BiOI. Therefore, BiOI/Bi_2WO_6 composite may be an ideal system to increase the photoabsorption property in the visible light region and to improve the separation efficiency of photogenerated charge carriers, and thus achieving a high photocatalytic performance.

In this work, BiOI/Bi_2WO_6 photocatalysts with different contents of BiOI were synthesized by a simple deposition method and characterized by X-ray diffraction (XRD), scanning electron microscopy (SEM), high-resolution transmission electron microscopy (HR-TEM), UV-Vis diffuse reflectance spectroscopy (UVVis DRS), and low temperature nitrogen adsorption. As the representative of organic pollutants, methyl orange and phenol were used to evaluate the photocatalytic activity and mechanism of BiOI/Bi_2WO_6 catalysts under UV and visible light irr adiation.

1 Experimental

1.1 Catalyst preparation

The pure Bi_2WO_6 sample was synthesized by a hydrothermal method according to previous studies[19-20]. The BiOI/Bi_2WO_6 catalysts with different BiOI contents were prepared by a deposition method. In a typical preparation, pure Bi_2WO_6 (1.0 g) was ultrasonically dispersed into deionized water to form a homogeneous mixture I. Different stoichiometric amounts of $Bi(NO_3)_3 \cdot 5H_2O$ (AR) and 0.03 g KI (AR) were dissolved in 20 mL ethylene glycol (AR) to obtain a clear solution II. Then the solution II was added dropwise into the mixture I under strong stirring for 5.0 h. The products were separated centrifugally, washed with absolute ethanol and deionized water, and dried at 353 K in air. The final BiOI/Bi_2WO_6 samples with various contents of BiOI are listed in Table 1.

1.2 Catalyst characterization

X-ray diffraction (XRD) were carried out on a Philips X′ pert diffractometer equipped with Ni-filtered Cu $K\alpha$ radiation source at a scanning speed of $2° \cdot min^{-1}$ from 20° to 70° (λ=0.154 18 nm). The X-ray tube was operated at 40 kV and 40 mA. X′ pert diffractometer with stationary tube and double goniometer system for point and line focus. The intensity was measured by a gas filled proportional detector. Scanning electron microscopy (SEM) images were recorded on an X-650 microscope operated at 25.0 kV. The BrunauerEmmettTeller (BET) surface area of catalysts was determined from N_2 adsorption isotherms at 77 K by a Micromeritics ASAP 2020 instrument. High-resolution transmission electron microscopy (HR-TEM) images and selected area

electron diffraction (SAED) were taken by a JEM-2100 electron microscope. The photoluminescence (PL) spectra with an excitation wavelength of 365 nm were recorded on a CARY Eclipse (America) fluorescence spectrophotometer. UV-Vis diffuse reflectance spectra of the samples were taken on a Shimadzu UV-3600 spectrophotometer (Japan).

1.3 Photoactivity measuement

The photocatalytic activity of $BiOI/Bi_2WO_6$ catalysts was evaluated by the degradation of methyl orange (MO) and phenol in an aqueous solution. The UV light was obtained by a 300 W high-pressure mercury lamp (λ_{max}=365 nm). The visible light source was a 400 W metal halide lamp (λ_{max} = 588 nm) with the combination of a cut-off filter (λ >400 nm) to eliminate UV radiation during visible light experiments. For each UV or visible light test, 45 mL MO (3.06×10^{-5} mol·L^{-1}) or phenol (1.06×10^{-4} mol·L^{-1}) aqueous solution and 0.06 g catalyst samples were used. A general procedure was as follows. First, MO or phenol aqueous solution was placed into a water-jacketed reactor maintained at 298 K, and then the catalyst samples were suspended in the solution. The suspension was stirred vigorously for 90 minutes in the dark to establish the adsorptiondesorption equilibrium of MO or phenol, then irradiated under UV or visible light. About 3.0 mL solution was withdrawn from the reactor periodically and centrifuged and analyzed for the degradation of MO and phenol using a TU-1901 spectrophotometer.

In order to study the effect of relevant reactive species, a quantity of different appropriate species quenchers was introduced into the photocatalytic degradation process of MO and phenol in a manner similar to the photodegradation experiment. The dosages of these species quenchers were adopted by reference to the previous literatures[21-22].

1.4 Recyle of the 13.2% $BiOI/Bi_2WO_6$ catalyst

The cleaned 13.2% $BiOI/Bi_2WO_6$ catalyst was immersed in ethanol for 5.0 h and rinsed with deionized water, and then dried at 353 K. After this, the cleaned 13.2% $BiOI/Bi_2WO_6$ catalyst was reused for the degradation of MO and phenol in an aqueous solution, and the recycle experiment was performed for five times.

2 Results and discussion

2.1 Catalyst structure

The crystal quality and structure of $BiOI/Bi_2WO_6$ samples were examined by XRD, and the results are shown in Fig.1. All diffraction peaks can be indexed to BiOI with a tetragonal crystal structure or Bi_2WO_6 with an orthorhombic crystal structure, which is agreed well with that of BiOI (PDF card No. 73-2062) and Bi_2WO_6 (PDF card No. 39-0256). When the amount of BiOI is lower than 7.10%, no significant diffraction peak of BiOI can be detected, which could be ascribed to its lower content and high dispersion on the surface of Bi_2WO_6 particles. The sharp and narrow diffraction peaks indicate that the samples are well crystallized. The average crystalline sizes of Bi_2WO_6 in the $BiOI/Bi_2WO_6$ composites are calculated from the (131) peaks, respectively, according to the Scherrer formula [23], and the results are listed Table 1.

The HR-TEM image of the 13.2% $BiOI/Bi_2WO_6$ sample is shown in Fig.2A. Clear fringe with an interval of 0.301 nm could be indexed to (012) lattice plane of tetragonal BiOI and that of 0.320 nm agreeing with the (131) lattice plane of orthorhombic Bi_2WO_6, which are in agreement with those of the XRD patterns in Fig.1. As shown in the corresponding SAED pattern (Fig.2B), diffraction spots with d values

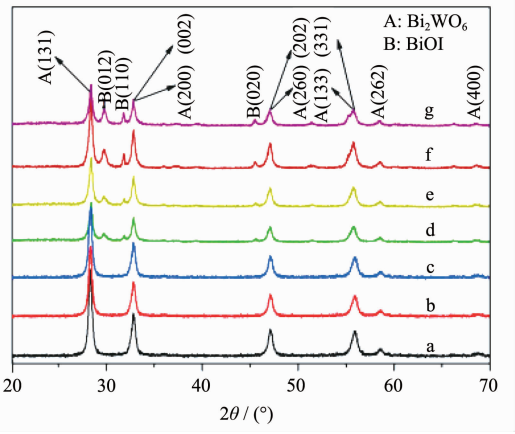

(a) 0.00; (b) 1.80; (c) 3.74; (d) 7.10; (e) 13.2; (f) 18.5; (g) 24.2

Fig.1 XRD patterns of $BiOI/Bi_2WO_6$ samples with different BiOI contents (wt%)

Table 1 The properties of BiOI/Bi_2WO_6 samples with different BiOI contents

BiOI content / wt%	Element (atomic composition %)				Average crystalline size / nm	BET surface area / ($m^2 \cdot g^{-1}$)
	Bi	O	I	W		
0.00	14.31	35.92	–	6.04	27.2	34
0.18	14.27	35.87	0.16	5.98	25.1	39
3.74	14.08	35.68	0.88	5.64	24.4	42
7.10	13.82	35.47	1.50	5.45	23.9	41
13.2	13.67	35.32	1.98	5.31	21.4	46
18.5	13.57	35.23	2.21	5.23	22.0	43
24.2	13.45	35.11	2.67	5.04	20.9	49

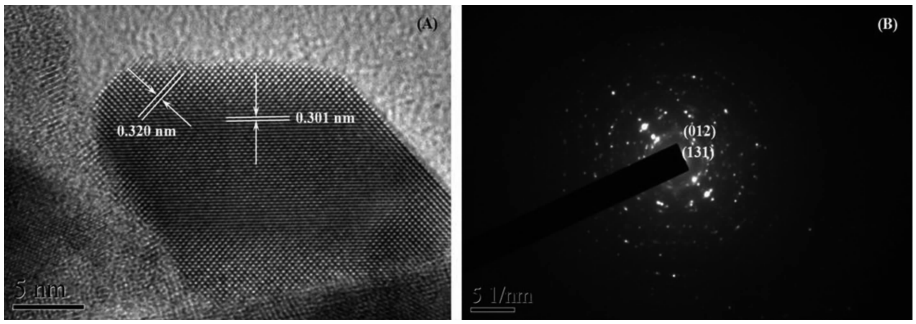

Fig.2 HR-TEM image (A) and SAED pattern (B) of the 13.2% BiOI/Bi_2WO_6 sample

of 0.316 and 0.304 nm are observed, which correspond to the (131) lattice plane of orthorhombic Bi_2WO_6 and (012) lattice plane of tetragonal BiOI, respectively. This could also be regarded as a proof for the coexistence of BiOI and Bi_2WO_6.

As revealed from Fig.3, with increasing BiOI content, the absorption intensity of BiOI/Bi_2WO_6 photocatalysts increases in the 380 ~600 nm light region and the absorption edge shifts significantly to longer wavelength as compared to pure Bi_2WO_6.

As a crystalline semiconductor, the optical absorption near the band edge follows the formula $\alpha h\nu = A(h\nu - E_g)^{n/2}$, where α, ν, E_g, and A are the absorption coefficient, light frequency, band-gap energy, and a constant, respectively[24]. For BiOI and Bi_2WO_6, the value of n is 4[24-25]. The band-gap energies (E_g values) of pure BiOI and Bi_2WO_6 could be thus estimated from a plot of $(\alpha h\nu)^{1/2}$ versus photon energy ($h\nu$). The intercept of the tangent to the x-axis will give a good approximation of the band-gap energies

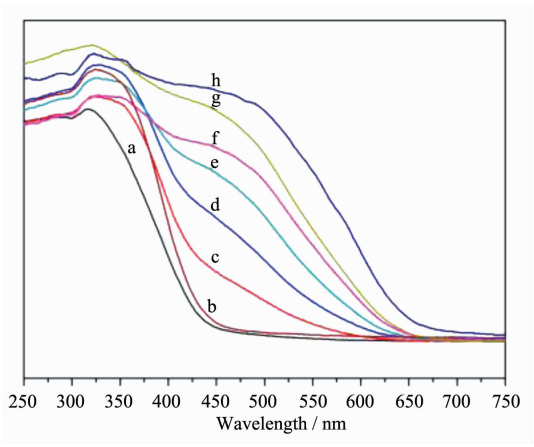

(a) 0.00; (b) 1.80; (c) 3.74; (d) 7.10; (e) 13.2; (f) 18.5; (g) 24.2; (h) 100

Fig.3 UV-Vis DRS of BiOI/Bi_2WO_6 samples with different BiOI contents (wt%)

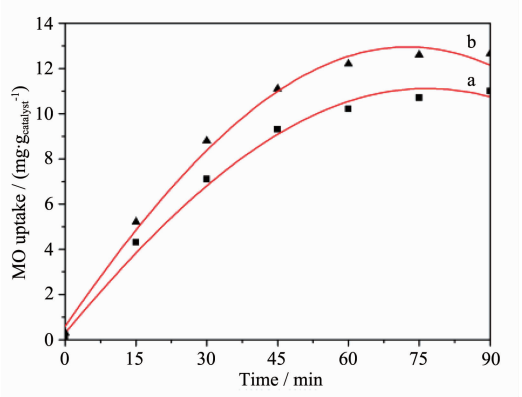

Fig.4 MO adsorptivity plot for (a) Bi_2WO_6 and (b) 13.2% BiOI/Bi_2WO_6 catalysts

for the pure BiOI and Bi_2WO_6 powders. The estimated E_g values are about 1.76 and 2.88 eV for pure BiOI and Bi_2WO_6, respectively, which are very close to the values reported [18,25-26]. The valence band (VB) edge position and the conduction band (CB) edge position of pure BiOI and Bi_2WO_6 at the point of zero charge were calculated by the formulas in the literatures[18,27], and the valence band potential (E_{VB}) of BiOI and Bi_2WO_6 are 2.32 and 3.30 eV, respectively, and the conduction band potential (E_{CB}) of BiOI and Bi_2WO_6 are 0.56 and 0.42 eV, respectively.

2.2 Adsorption studies

The activity of photocatalyst is related to its adsorbability [28-29]. Hence, the research of MO adsorption was performed on Bi_2WO_6 and 13.2% BiOI/Bi_2WO_6 catalysts using 0.012 g of catalyst at room temperature in the dark. The adsorption capacity of Bi_2WO_6 and 13.2% BiOI/Bi_2WO_6 catalysts is shown in Fig.4. The adsorption behaviors of MO on Bi_2WO_6 and 13.2% BiOI/Bi_2WO_6 catalysts follow the Langmuir model.

It could be seen that MO uptake capacity moderately increases in the presence of the 13.2% BiOI/Bi_2WO_6 catalyst compared with that of Bi_2WO_6 catalyst. The adsorbed quantities of MO, q_t (mg·$g_{catalyst}^{-1}$), at time t are calculated by equation (**1**):

$$q_t = [(C_0 - C_t) \times 1\ 000 \times M_W \times V_0]/w_{catalyst} \quad (1)$$

where C_0 and C_t (mol·L^{-1}) are the initial concentration and concentration (g·mol^{-1}) at time t of MO, respectively; M_W is the molecular weight of MO; V_0 is the volume of MO aqueous solution (L); and $w_{catalyst}$ is the mass of the catalyst (g). The equilibrium adsorption capacity (q_e) is usually estimated by the pseudo-first-order and pseudo-second-order model, and the correct values are chosen by the higher coefficient of determination R^2. [30]. Here, the equilibrium adsorption capacity (q_e) of Bi_2WO_6 and 13.2% BiOI/Bi_2WO_6 catalysts is 10.95 and 12.60 mg·$g_{catalyst}^{-1}$, respectively. Clearly, the adsorption ability of Bi_2WO_6 is enhanced by introduction of BiOI, which is of benefit to increase the photocatalytic performance[31-32].

2.3 Photocatalytic activity

The effect of BiOI content on the UV and visible light photocatalytic activities of BiOI/Bi_2WO_6 was investigated by MO degradation in an aqueous solution, and the results are shown in Fig.5. Under UV and visible light irradiation, the self-degradation of MO is negligible in the absence of catalyst, indicating that the photolysis could be ignored. However, in the presence of catalysts, the irradiation of UV and visible light could result in the obvious degradation of MO. The BiOI content in the Bi_2WO_6 exerts great influences on the UV and visible light photocatalytic activity of BiOI/Bi_2WO_6 catalyst. With BiOI content increasing, the UV and visible light photocatalytic activity of BiOI/Bi_2WO_6 first increases, reaching a maximum at BiOI content of 13.2% , and then decreases with further increasing BiOI content, which could be attributed to the fact that the excessive BiOI with narrow band gap would be acted as the recombination center of electrons and holes[26],

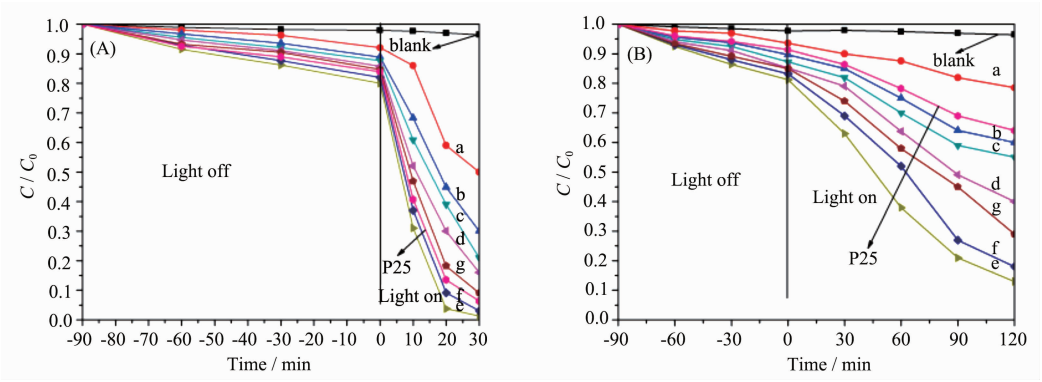

(a) 0.00; (b) 1.80; (c) 3.74; (d) 7.10; (e) 13.2; (f) 18.5; (g) 24.2

Fig.5　Effect of the BiOI content (wt%) in the BiOI/Bi_2WO_6 catalysts on the degradation of MO under UV

impeding negative effect on the photocatalytic activity. The 13.2% BiOI/Bi_2WO_6 catalyst has obviously higher UV (98.7%) and visible (87.0%) light photocatalytic activity than P25 (UV: 93.7%, Vis: 36%) and Bi_2WO_6 (UV: 50.1%, Vis: 21.5%), indicating that introduction of BiOI in the Bi_2WO_6 with optimum BiOI content remarkably enhances the UV and visible light photocatalytic activity of Bi_2WO_6.

Chemical Oxygen Demand (COD) refers to the oxidative decomposition of the oxidizable substances (such as organics, nitrite, ferrous salts, sulfides, etc.) in the water through chemical oxidants such as potassium permanganate, the oxygen consumption is then calculated according to the amount of the residual oxidant.

In order to confirm that the decolorization of MO is really originated from the photocatalysis, the percentage change of COD which reflects the extent of degradation or mineralization of organic species is studied as a function of irradiation time in the photodegradation of MO under UV (a) and visible (b) light irradiation, as shown in Fig.6. If the MO dye is not degraded completely, the residual colorless organic molecules could be oxidized by $K_2Cr_2O_7$; thus, the oxygen demand will be higher. The initial COD concentration of the MO solution is 38.5 mg·L^{-1}. After 120 min UV and visible light irradiation, the COD concentration decreases to 5.4 and 18.6 mg·L^{-1}, respectively. The reduction of COD value further confirms that MO is truly photodegraded by the 13.2% BiOI/Bi_2WO_6 photocatalyst.

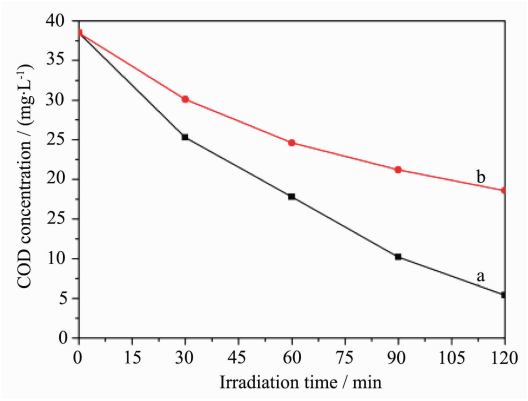

(A) (λ_{max}=365 nm) and visible (B) (λ_{max}=588 nm) light irradiation

Fig.6 Variation of COD of MO aqueous solutions treated with 13.2% BiOI/Bi_2WO_6 under UV (a) and visible (b) light irradiation

Fig.7 shows the photocatalytic degradation of phenol as a function of irradiation time with BiOI/Bi_2WO_6 samples under UV (A) and visible (B) light irradiation. It could be seen that the decrease of phenol concentration with blank and pure Bi_2WO_6 is very small.

Obviously, the BiOI/Bi_2WO_6 composite exhibits much higher photodegradation efficiency than pure Bi_2WO_6. The reduction of phenol is about 61.0% and 19.0% after 30 min UV and 120 min visible light irradiation in the presence of P25 sample, respectively. In our result, the 13.2% BiOI/Bi_2WO_6 sample presents the best photocatalytic activity, with the reduction of phenol concentration as much as 71.0% and 57.0%, respectively, under the same

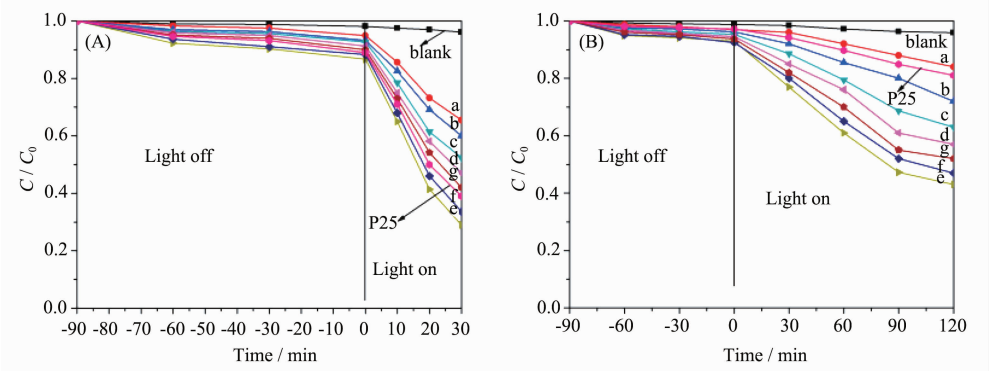

(a) 0.00; (b) 1.80; (c) 3.74; (d) 7.10; (e) 13.2; (f) 18.5; (g) 24.2

Fig.7 Effect of BiOI content (wt%) in the BiOI/Bi_2WO_6 catalysts on the degradation of phenol under UV (A) (λ_{max}=365 nm) and visible (B) (λ_{max}=588 nm) light irradiation

experimental conditions.

In order to confirm the advantage of heterojunction between BiOI and Bi_2WO_6, 13.2% BiOI/Bi_2WO_6 was compared with the mechanical mixture of BiOI and Bi_2WO_6 with the similar composition under identical experimental conditions. The results have shown that the 13.2% BiOI/Bi_2WO_6 catalyst (deposition method) has obviously higher UV (MO: 98.7%; phenol: 71.0%) and visible (87.0%; phenol: 57.0%) light photocatalytic activity than 13.2% BiOI/Bi_2WO_6 (Mechanically mixed) (MO: 88.7%; phenol: 56.6%) and (MO: 68.9%; phenol: 45.3%), respectively. Clearly, the UV and visible light photocatalytic activities of mechanically mixed 13.2% BiOI/Bi_2WO_6 are lower than that of 13.2% BiOI/Bi_2WO_6 synthesized by deposition method. This is mainly because BiOI and Bi_2WO_6 behave as independent catalysts rather than a coupled system in the mechanical mixture of BiOI and Bi_2WO_6, which is unfavorable to the transfer of charge carriers from one phase to another. The results exhibit that the BiOI and Bi_2WO_6 heterojunction fabricated in the BiOI/Bi_2WO_6 sample could improve the UV and visible light photocatalytic activities obviously.

Fig.8 shows the recycling activity of the 13.2% BiOI/Bi_2WO_6 catalyst for the photocatalytic degradation of MO and phenol. It can be seen that the photocatalytic activity of the sample shows a certain extent decrease with increasing recycling times, which may be due to the mass loss during the sedimentation and transferring processes and the gradually decline in adsorptive capacity of the catalyst[33].

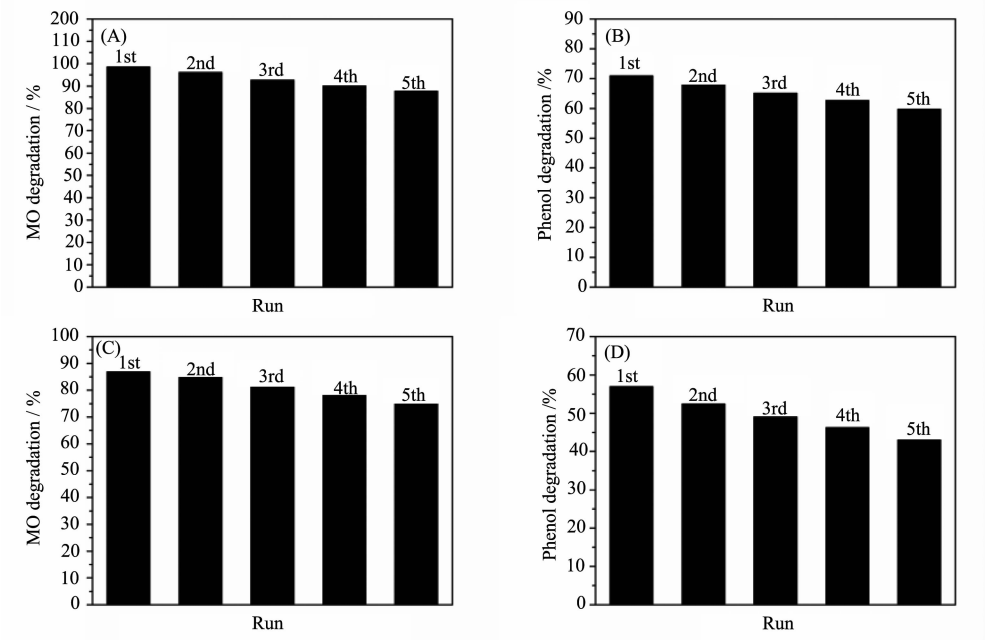

Fig.8 Photocatalytic degradation of MO and phenol in the presence of 13.2% BiOI/Bi_2WO_6 catalyst by reuse under UV (A, B) and visible (C, D) light irradiation

2.4 Discussion of photocatalytic mechanism

The photocatalytic results have shown that BiOI/Bi_2WO_6 catalysts have excellent photocatalytic activities on the degradation of MO and phenol. Therefore, it is necessary to discuss the photocatalytic mechanism for MO and phenol over the title catalyst.

2.4.1 Reactive species involved in the photocatalytic process

The effect of various radical scavengers on the degradation of MO and phenol under UV and visible light irradiation were performed to study the underlying photodegradation mechanism of pure Bi_2WO_6 and 13.2% BiOI/Bi_2WO_6 catalysts. Isopropanol (IPA)[21,34], as an ·OH scavenger, was added to the reaction system, and benzoquinone (BQ)[21,35] was introduced as the scavenger of $\cdot O_2^-$. To investigate the role of H_2O_2 and h^+ radical species, catalase (CAT)[21] and ammonium oxalate (AO)[36] were also added to the

reaction system, respectively. The results are shown in Fig.9. When the radical species play a major role in the degradation of MO or phenol, the degradation efficiency (k_{app}) of pure Bi_2WO_6 and 13.2% BiOI/Bi_2WO_6 catalysts will be expected to decrease obviously.

It can be seen from Fig.9 that the degradation efficiency for MO and phenol over pure Bi_2WO_6 and 13.2% BiOI/Bi_2WO_6 catalysts under UV and visible light irradiation decreases significantly after the addition of IPA, BQ, AO and CAT, respectively, compared with no scavenger under the identical conditions, i.e. under UV and visible light irradiation, ·OH, $\cdot O_2^-$, h^+ and H_2O_2, especially h^+, together dominate the photodegradation process of MO and phenol.

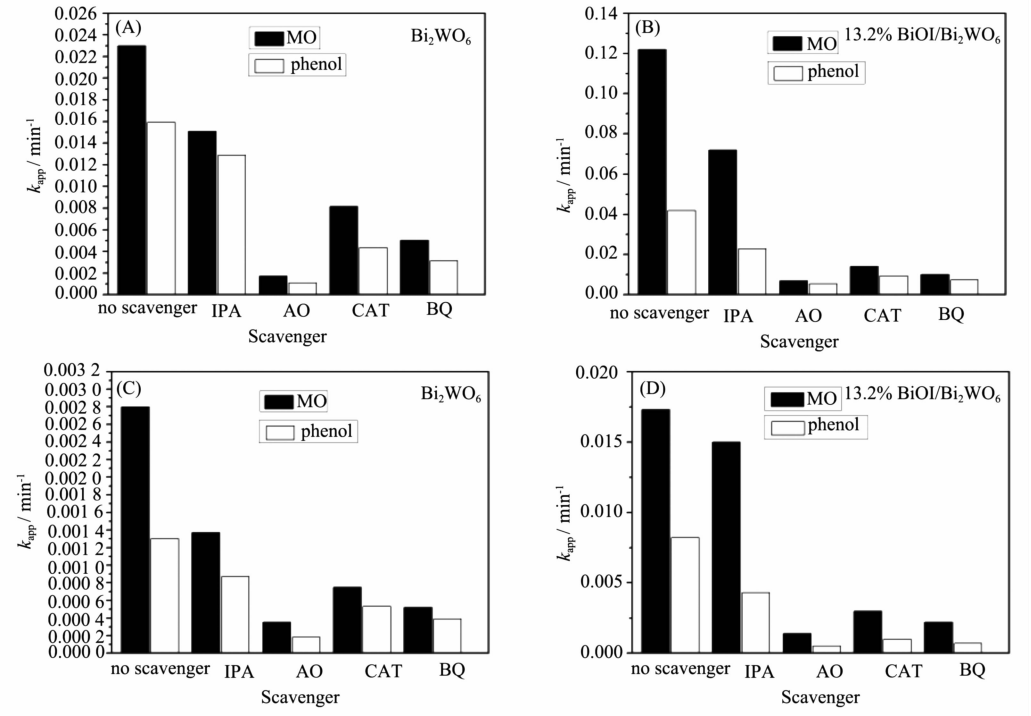

Fig.9 Effects of different scavengers on the degradation of MO and phenol over Bi_2WO_6 and 13.2% BiOI/Bi_2WO_6 under UV (A, B) and visible (C, D) light irradiation

2.4.2 Origin of reactive species for MO and phenol degradation

Taking into account the kinds of reactive species in the MO and phenol degradation, the photocatalytic process of pure Bi_2WO_6 and 13.2% BiOI/Bi_2WO_6 catalysts could be described as follows (Eqs.(**2**)~(**11**)):

$$\text{Catalyst}+h\nu \rightarrow e^-+h^+ \quad (\mathbf{2})$$

$$e^-+O_2 \rightarrow \cdot O_2^- \quad (\mathbf{3})$$

$$e^-+O_2+2H^+ \rightarrow H_2O_2 \quad (\mathbf{4})$$

$$H_2O_2+e^- \rightarrow \cdot OH+OH^- \quad (\mathbf{5})$$

$$H_2O+h^+ \rightarrow \cdot OH+H^+ \quad (\mathbf{6})$$

$$OH^-+h^+ \rightarrow \cdot OH \quad (\mathbf{7})$$

$$\text{MO and phenol}+\cdot O_2^- \rightarrow \text{products} \quad (\mathbf{8})$$

$$\text{MO and phenol}+H_2O_2 \rightarrow \text{products} \quad (\mathbf{9})$$

$$\text{MO and phenol}+\cdot OH \rightarrow \text{products} \quad (\mathbf{10})$$

$$\text{MO and phenol}+h^+ \rightarrow \text{products} \quad (\mathbf{11})$$

In the above process, electronhole pairs are directly produced by photocatalyst after UV or visible light illumination. Then, the photogenerated electrons transfer to CB bottom of the catalyst and react with the adsorbed O_2 on the surface of catalyst to form $\cdot O_2^-$, H_2O_2 and ·OH that could oxidize MO and phenol. At the same time, the holes are left on the VB top, reacting with the adsorbed H_2O or OH^- on the surface of catalyst to form ·OH that could also oxidize MO and phenol, or the holes react directly with MO and phenol.

2.4.3 Photocatalytic activity enhancement mechanism of BiOI/Bi_2WO_6

Using two semiconductors in contact with different redox energy levels of conduction band and valence band could be used to improve

photogenerated carriers separation and to enhance the efficiency of the interfacial charge transfer [37]. The valence band (VB) edge position and the conduction band (CB) edge position of BiOI and Bi_2WO_6 are estimated by the following formulas[17,27]:

$$E_{VB} = X - E^e + 0.5E_g$$

$$E_{CB} = E_{VB} - E_g$$

where E_{VB} and E_{CB} are the valence band (VB) potential and conduction band (CB) potential, respectively. X is the electronegativity of BiOI or Bi_2WO_6, and the X values of BiOI and Bi_2WO_6 are 5.943 and 6.363 eV, respectively. E^e is the energy of free electrons on the hydrogen scale (~4.5 eV) and E_g is the band gap energy of BiOI or Bi_2WO_6. Here, the E_{VB} values of BiOI and Bi_2WO_6 are 2.32 and 3.30 eV, respectively. The E_{CB} values of BiOI and Bi_2WO_6 are 0.56 and 0.42 eV, respectively. As shown in Fig.10, when p-type BiOI and n-type Bi_2WO_6 are contacted, the Fermi level of p-type BiOI moves up, at the same time, that of n-type Bi_2WO_6 moves down until the equilibrium state is formed [38]. Consistent with the moving of the Fermi level, the whole energy band of p-type BiOI raises up, while that of n-type Bi_2WO_6 descends. An inner electric field from n-type Bi_2WO_6 to p-type BiOI is thus formed. Under UV or visible-light irradiation, both BiOI and Bi_2WO_6 could be excited to generate electron-hole pairs. According to the energy-band schematic diagram shown in Fig.10, the photogenerated electrons on the conduction band of p-type BiOI could transfer to that of n-type Bi_2WO_6, while simultaneously photogenerated holes could migrate from the valence band of n-type Bi_2WO_6 to that of p-type BiOI. Such migrations of the photogenerated carriers could be promoted by the internally formed electric field. Therefore, the photogenerated electrons and holes could be separated effectively owing to formation of the p-n junction between p-type BiOI and n-type Bi_2WO_6 interfaces[39]. The better separation of electrons and holes in the $BiOI/Bi_2WO_6$ catalysts could be also confirmed by photoluminescence (PL) emission spectra of Bi_2WO_6 and 13.2% $BiOI/Bi_2WO_6$ samples (Fig.11).

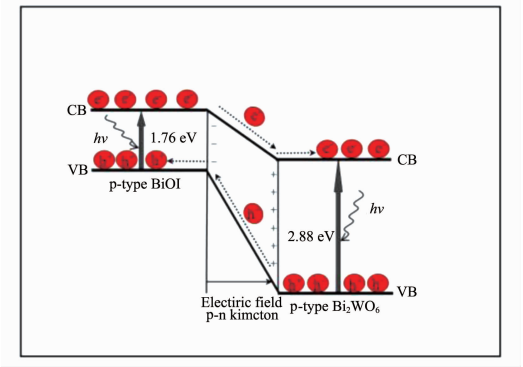

Fig.10　Diagram of photoinduced e/h^+ pairs transfer of Bi_2WO_6 and BiOI

PL emission spectra have been widely used to investigate the separation efficiency of the photogenerated charge carriers in a semiconductor[40-42]. The comparison of PL spectra (excited at 365 nm) of Bi_2WO_6 and 13.2% $BiOI/Bi_2WO_6$ samples at room temperature is shown in Fig.11. It can be seen that Bi_2WO_6 and 13.2% $BiOI/Bi_2WO_6$ have a broad emission peak, and the strongest emitting peaks around 469 nm are similar, while PL emission intensity of the 13.2% $BiOI/Bi_2WO_6$ sample was dramatically weakened compared with that of Bi_2WO_6, indicating that the recombination of photogenerated charge carriers is greatly inhibited by the BiOI introduction. In other words, an appropriate amount of BiOI in the Bi_2WO_6 is helpful to separate the photogenerated charge carriers, and then improve the UV and visible light photocatalytic activity of $BiOI/Bi_2WO_6$ samples.

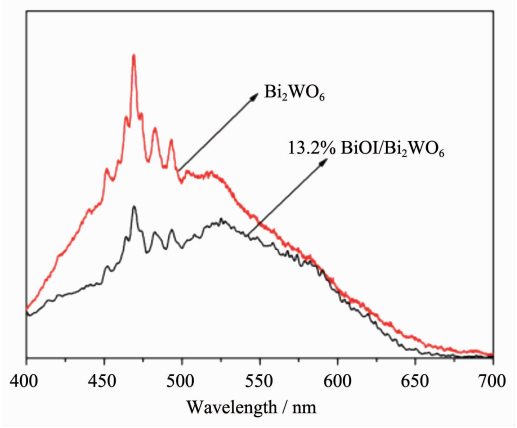

Fig.11　PL spectra of Bi_2WO_6 and 13.2% $BiOI/Bi_2WO_6$ samples recorded at room temperature

3　Conclusions

In summary, the $BiOI/Bi_2WO_6$ photocatalysts with

different BiOI contents were prepared by a simple deposition method. Under UV and visible light irradiation, the photocatalytic activity of 13.2% BiOI/Bi_2WO_6 is much higher than those of commercial Degussa P25 and pure Bi_2WO_6 toward MO and phenol. The obviously improved properties could be mainly attributed to the enhancement of electron-hole separations at the interface of Bi_2WO_6 and BiOI. Radical scavengers experiments demonstrate that ·OH, h^+, $\cdot O_2^-$ and H_2O_2, especially h^+, together dominate the photodegradation process of MO and phenol.

Acknowledgments: This work was supported by the National Natural Science Foundation of China (21201037) and Natural Science Foundation of Higher Education Institutions in Anhui Province (KJ2012A217) and school-level program (2013HJJC01ZD) of Anhui Provincical Key Laboratory for Degradation and Monitoring of Pollution of the Environment.

References:

[1] Chen X B, Liu L, Yu P Y, et al. *Science*, **2011**,**331**(6018):746-750

[2] Mills A, Hazafy D. *Chem. Commun.*, **2012**,**48**(4):525-527

[3] Oncescu T, Stefan M I, Oancea P. *Environ. Sci. Pollut. Res.*, **2010**,**17**(5):1158-1166

[4] LI Hui-Quan(李慧泉), CUI Yu-Min(崔玉民), WU Xing-Cai(吴兴才), et al. *Chinese J. Inorg. Chem.* (无机化学学报), **2012**,**28**(12):2597-2604

[5] Sério S, Jorge M E M, Coutinho M L, et al. *Chem. Phys. Lett.*, **2011**,**508**(1/2/3):71-75

[6] Nonoyama T, Kinoshita T, Higuchi M, et al. *J. Am. Chem. Soc.*, **2012**,**134**(21):8841-8847

[7] Chen S F, Zhang S J, Liu W, et al. *J. Hazard. Mater.*, **2008**, **155**(1/2):320-326

[8] Li Y Z, Fan Y N, Chen Y. *J. Mater. Chem.*, **2002**,**12**(5):1387-1390

[9] Carretero-Genevrier A, Boissiere C, Nicole L, et al. *J. Am. Chem. Soc.*, **2012**,**134**(26):10761-10764

[10]Obregón Alfaro S, Martínez-de la Cruz1 A. *Appl. Catal. A: Gen.*, **2010**,**383**(1/2):128-133

[11]Mann A K P, Skrabalak S E. *Chem. Mater.*, **2011**,**23**(4):1017-1022

[12]Wu D X, Zhu H T, Zhang C Y, et al. *Chem. Commun.*, **2010**, **46**(38):7250-7252

[13]Amano F, Nogami K, Tanaka M, et al. *Langmuir*, **2010**,**26**(10):7174-7180

[14]Huang Y, Ai Z, Ho W, et al. *J. Phys. Chem. C*, **2010**,**114**(14):6342-6349.

[15]Min Y L, Zhang K, Chen Y C, et al. *Sep. Purif. Technol.*, **2012**,**92**(5):115-120

[16]Xiao Q, Zhang J, Xiao C, et al. *Catal. Commun.*, **2008**,**9**(6):1247-1253

[17]Zhang X, Zhang L Z, Xie T F, et al. *J. Phys. Chem. C*, **2009**,**113**(17):7371-7378

[18]Chen L, Yin S F, Luo S L, et al. *Ind. Eng. Chem. Res.*, **2012**,**51**(19):6760-6768

[19]Li H Q, Cui Y M, Hong W S. *Appl. Surf. Sci.*, **2013**,**264**(1):581-588

[20]Zhang Z J, Wang W Z, Wang L, et al. *Appl. Mater. Interfaces*, **2012**,**4**(2):593-597

[21]Li G T, Wong K H, Zhang X W, et al. *Chemosphere*, **2009**, **76**(9):1185-1191

[22]Cao J, Xu B Y, Luo B D, et al. *Catal. Commun.*, **2011**,**13**(1):63-68

[23]Galceran M, Pujol M C, Zaldo C, et al. *J. Phys. Chem. C*, **2009**,**113**(35):15497-15506

[24]Zhang X, Ai Z H, Jia F L, et al. *J. Phys. Chem. C*, **2008**, **112**(3):747-753

[25]Song X C, Zheng Y F, Ma R, et al. *J. Hazard. Mater.*, **2011**,**192**(1):186-191

[26]Cao J, Xu B Y, Lin H L, et al. *Chem. Eng. J.*, **2012**,**185/186**(6):91-97

[27]Zhang L, Wang W Z, Zhou L, et al. *Appl. Catal. B: Environ.*, **2009**,**90**(3/4):458-462

[28]Chen X, Mao S S. *Chem. Rev.*, **2007**,**107**(7):2891-2959

[29]Chen S F, Liu Y Z. *Chemosphere*, **2007**,**67**(5):1010-1017

[30]Kangwansupamonkon W, Jitbunpot W, Kiatkamjornwong S. *Polym. Degrad. Stabil.*, **2010**,**95**(9):1894-1902

[31]Zhang H. Lü X J, Li Y M, et al. *ACS Nano*, **2008**,**2**(7):1487-1491

[32]Morales W, Cason M, Aina O, et al. *J. Am. Ceram. Soc.*, **2008**,**130**(20):6318-6319

[33]Hao R, Xiao X, Zuo X X, et al. *J. Hazard. Mater.*, **2012**, **209/210**(5):137-145

[34]Zhang L S, Wong K H, Yip H Y, et al. *Environ. Sci. Technol.*, **2010**,**44**(4):1392-1398

[35]Yin M C, Li Z S, Kou J H, et al. *Environ. Sci. Technol.*, **2009**,**43**(21):8361-8366

[36]Zhang N, Liu S Q, Fu X Z, et al. *J. Phys. Chem. C*, **2011**, **115**(18):9136-9145

[37]Helali N, Bessekhouad Y, Bouguelia A, et al. *J. Hazard. Mater.*, **2009**,**168**(1):484-492

[38]Li X N, Huang R K, Hu Y H, et al. *Inorg. Chem*., **2012**,**51**(11):6245-6250

[39]Guan M L, Ma D K, Hu S W, et al. *Inorg. Chem.*, **2011**,**50**(3):800-805

[40]Tang J W, Zou Z G, Ye J H. *J. Phys. Chem. B*, **2003**,**107**(51):14265-14269

[41]Yu J G, Yu H G, Cheng B, et al. *J. Phys. Chem. B*, **2003**, **107**(50):13871-13879

[42]Jing L Q, Qu Y C, Wang B Q, et al. *Sol. Energy Mat. Sol. Cells*., **2006**,**90**(12):1773-1787